MICROBIAL ECOLOGY

Microb Ecol (2000) 40:94–103
DOI: 10.1007/s002480000061

Bio-optical Characteristics and the Vertical Distribution of Photosynthetic Pigments and Photosynthesis in an Artificial Cyanobacterial Mat

M. Kühl, T. Fenchel

Marine Biological Laboratory, University of Copenhagen, Strandpromenaden 5, DK-3000 Helsingør, Denmark

Received: 20 December 1999; Accepted: 10 June 2000; Online Publication: 28 August 2000

Abstract

Zonations of photosynthesis and photopigments in artificial cyanobacterial mats were studied with (i) oxygen and pH microsensors, (ii) fiber-optic microprobes for field radiance, scalar irradiance, and PSII fluorescence, and (iii) a light microscope equipped with a spectrometer for spectral absorbance and fluorescence measurements. Our analysis revealed the presence of several distinct 1–2 mm thick cyanobacterial layers mixed with patches of anoxygenic photosynthetic bacteria. Strong attenuation of visible light confined the euphotic zone to the uppermost 3 mm of the mat, where oxygen levels of 3–4 times air saturation and a pH peak of up to pH 8.8 were observed under saturating irradiance (413 μmol photon m^{-2} s^{-1}). Oxygen penetration was 5 mm in light and decreased to 1 mm in darkness. Volumetric oxygen consumption in the photic and aphotic zones of illuminated mat was 5.5 and 2.9 times higher, respectively, than oxygen consumption in dark incubated mats. Scalar irradiance reached 100–150% of incident irradiance in the upper 0.5 mm of the mat due to intense scattering in the matrix of cells, exopolymers, and carbonate precipitates. In deeper mat layers scalar irradiance decreased nearly exponentially, and highest attenuation coefficients of 6–7 mm^{-1} were found in cyanobacterial layers, where photosynthesis and photopigment fluorescence also peaked. Visible light was attenuated >100 times more strongly than near infrared light. Microscope spectrometry on thin sections of mats allowed detailed spectral absorbance and fluorescence measurements at defined positions relative to the mat surface. Besides strong spectral signals of cyanobacterial photopigments (Chl *a* and phycobiliproteins), the presence of both green and purple photosynthetic bacteria was evident from spectral signals of Bchl *a* and Bchl *c*. Microprofiles of photopigment absorbance correlated well with microdistributions of phototrophs determined in an accompanying study.

Correspondence to: Michael Kühl; Fax: +45 49261165; E-mail: mblmik@inet.uni2.dk

Introduction

Photosynthetic microbial mats occur as complex, macroscopically relatively homogeneous, stratified microbial communities in light exposed habitats, where bioturbation and grazing are minimal or even absent because of extremes of one or more environmental parameters, e.g., high salinity or temperature, low water activity, or high levels of toxic hydrogen sulfide. Such microbial mats are often used as model systems to study microbial interactions and biogeochemical processes (e.g. [41]. Further interest in microbial mats is due to a pronounced similarity between some microbial mats and preserved biogenic structures, stromatolites, in the fossil record [36, 37, 43]. Based on stable carbon isotopic signatures [34] and the presence of microfossils with a striking similarity especially to cyanobacteria [36], which are dominant in present microbial mats, stromatolites are regarded as the oldest autotrophic communities on Earth. Microbial mats are thus viewed as recent analogues to stromatolites, and biogeochemical and microbiological studies of microbial mats are often used to infer or hypothesize about the function of the earliest microbial communities on Earth [32].

Most microbial mat research has focused on well-developed mats in extreme environments, and, especially, the structure and function of microbial mats found in hypersaline or geothermal habitats has been studied intensively for >25 years (see [3, 5, 32, 38, 44, 45] for recent reviews). Less effort has been spent on studying the formation and structure of microbial mats in temperate coastal environments [28, 30, 31, 39, 42]. To our knowledge, the first direct demonstration that removal of fauna in natural coastal sediments can induce the formation of laminated microbial mats both similar in structure and function to mats found in extreme environments, was presented by Fenchel in a series of papers [8–10]. Here we present an investigation of the light field and the distribution of photosynthesis and photopigments in such artificial cyanobacterial mats, as measured by microsensors in intact mat samples and by microspectrometry on thin sections of mats. In an accompanying paper [11] a detailed light and transmission electron microscopic analysis of the mat structure and microbial composition is presented.

Materials and Methods

Experimental Setup

The microbial mat used in this study had developed with an accretion rate of 2–3 mm per year on experimentally defaunated sediment cores kept in aerated sterile seawater under an experimental 14 h light: 10 h dark cycle since 1996 [8, 11]. The experiments were done with approximately 2.6-year-old mats with a thickness of ca 7 mm on top of the sediment. Details on growth rate, structure and the vertical zonation of the biota as inferred from microscopy can be found in [11].

Microsensor measurements were done at room temperature (20°C) on mat samples mounted in a small black Plexiglas core (25 mm height; 20 mm width), which was used for subcoring a larger sample in the mat incubation setup. Prior to measurements, the mat surface was adjusted flush with the upper side of the core and then positioned in a small flow chamber originally presented by Lorenzen et al. [27]. The sample was embedded in agar, only leaving the mat surface exposed to the flow of aerated seawater (salinity: 22‰), which was circulated through the flow chamber by a water pump (Eheim, Germany) submerged in a larger reservoir of aerated seawater.

The mat was illuminated vertically from above with a fiber-optic tungsten-halogen lamp (KL-1500, Schott, Germany) equipped with a collimating lens. The heat filter of the lamp was removed to allow for both visible and near infrared illumination. Different experimental irradiances were obtained with the help of neutral density filters. The incident irradiance (= downwelling scalar irradiance for vertically incident collimated light) in the setup was calibrated prior to the experiments by positioning a scalar irradiance meter (QSL-101, Biospherical Instruments, USA) over a black light well, which was placed in the light path at an identical position and with the same amount of overlying water as the mat sample. Experimental light–dark shifts were created with an electronic shutter inserted in the light path between the lamp and the mat surface.

Microsensors were mounted in a micromanipulator (Märtzhäuser, Germany) equipped with a motor (Encoder Mike, LOT-Oriel Germany). The microsensors penetrated the mat at a zenith angle of 145° relative to the vertical. In the following, all depths have been corrected for the insertion angle and are given in units of vertical distance below or above the mat surface. Positioning, light control, and data acquisition of the microsensor signals was done with custom software (Pyro Imagination, Denmark). The surface position of the microsensors, where the measuring tip just touched the diffuse ~0.5–1 mm thick upper layer of the mat, was determined visually under a dissection microscope. Our depth scale thus includes the mucous surface layer as part of the mat.

Microsensor Measurements

Microprofiles of oxygen and oxygenic photosynthesis were measured with fast responding (t_{90} <0.3 s) Clark-type oxygen microsensors [33] equipped with a guard electrode and connected to a sensitive picoamperemeter (Unisense Aps, Denmark). The microsensors were linearly calibrated from readings in the air-saturated seawater of known salinity (22‰) and temperature (20°C) above the mat and from readings in the anoxic part of the mat. Gross photosynthesis and net fluxes of oxygen in the light (net photosynthesis) and in dark (dark respiration) were measured as previously described [21]. For flux calculations we used an oxygen dif-

fusion coefficient in water, D_0, of 2.03×10^{-5} cm^2 s^{-1}, as calculated for 20°C and 22‰ salinity [1, 26]. The porosity, ϕ, of the mat was assumed to be 0.95, and we assumed a constant oxygen diffusivity in the mat of $\phi D_s = 0.7\ D_0 = 1.42 \times 10^{-5}$ cm^2 s^{-1} [14].

Microprofiles of pH were measured with glass pH microelectrodes connected to a high-impedance millivoltmeter and a standard calomel reference electrode. The pH microelectrodes were calibrated at experimental temperature with standard buffers (Radiometer, Denmark) and exhibited a slope of the calibration curve of 55–59 mV per pH unit.

Microprofiles of diffuse backscattered field radiance and of quantum scalar irradiance were measured with fiber-optic microprobes [20]. Spectral measurements of backscattered field radiance (145° zenith angle), $L_u(\lambda)$, were done with the field radiance microprobe connected to a sensitive diode array spectrometer with a spectral range of 300–800 nm (PMA-11, Hamamatsu Photonics, Japan). Raw spectra were corrected for dark current and varying exposure time and then normalized to reflection spectra measured over a $BaSO_4$ reflection standard with a flat spectral reflectance of >98% over 400–900 nm light (LabLeader White Reflectance standard, Eastman-Kodak, USA). The reflectance standard was positioned at the same position in the light path as the mat surface.

Measurements of integral quantum scalar irradiance from 400 to 700 nm, E_0(PAR), were done with a previously described measuring system [22]. The same paper describes technical details of calibration and measurement. Depth profiles of the diffuse attenuation coefficients of E_0(PAR) were calculated as

$$K_0(z) = -\mathrm{d}(\ln E_0)/\mathrm{d}z$$

by use of the derivative function of Origin 6.0 (Microcal Software Inc., USA) with log transformed depth profiles of E_0(PAR).

Microprofiles of chlorophyll *a* and phycobiliprotein fluorescence were measured with tapered field radiance microprobes (tip diameter 30–40 μm) [20] connected either to a custom-built fiber-optic fluorometer with a lock-in amplifier (Roland Thar et al., unpublished) or to a commercially available pulse amplitude modulated fluorometer (Microfiber PAM, Walz GmbH, Germany; [35]). Because of signal modulation, both instruments allow for measurements of weak fluorescence signals on a high background of ambient light. Both fluorometers use LED light sources for excitation and a photomultiplier for detection. Depending on the choice of excitation wavelengths (i.e., LED type + short-pass filter) and of the long-pass or band-pass filters positioned in front of the detector, the fluorescence of different photopigments can be discriminated. For Chl *a* fluorescence we used blue excitation at 450 nm and detected red fluorescence at 650–750 nm. For phycobiliprotein fluorescence we used orange excitation at 590 nm and detected red fluorescence at 650–750 nm. At normal temperatures chlorophyll fluorescence from living cells originates primarily from PSII and its associated antenna pigments [16].

Microscope Spectrometry

Fine-scale measurements of spectral absorbance and fluorescence were also done on vertical thin sections obtained by freeze-sectioning the microbial mat (described in [11]). Each section had a thickness of ~30–40 μm and spanned the upper 4–5 mm of the mat. The mounted sections were investigated on an epifluorescence microscope with a camera mounted on a phototubus (Olympus, Japan). For spectral measurements, a fiber-optic cable connected to a diode array spectrometer replaced the camera. We used both a Hamamatsu PMA-11 spectrometer (300–800 nm) (Hamamatsu Photonics, Japan) and a small Zeiss MMS-1 spectrometer module (300–900 nm) (Zeiss, Germany), which was equipped with a preamplifier (Cronin GmbH, Germany). For absorbance measurements, a fiber-optic halogen lamp without a heat filter (KL-1500, Schott, Germany) was coupled into the microscope instead of the normal halogen lamp. For fluorescence measurements, the mercury arc lamp of the microscope was used in combination with the microscope filters for blue excitation and red fluorescence. By limiting the field of view with an iris diaphragm, spot measurements of spectral absorbance or fluorescence could be done at 40–200 μm resolution at specific locations of the vertical thin section, which were documented by photography beforehand [11]. Vertical profiles of absorbance and fluorescence were obtained by systematically scanning the vertical section from the surface layer and downwards in steps of 200 μm. Reference spectra of incident light and background fluorescence were measured in areas with no mat present and, subsequently, used to correct the raw spectra obtained at different locations on the thin section. Spectral absorbance, $A(\lambda)$, was estimated from

$$A(\lambda) = \log\left(I_0(\lambda)/I(\lambda)\right)$$

where $I_o(\lambda)$ is the incident light intensity and $I(\lambda)$ the transmitted light intensity at a specific wavelength, λ. We estimated I_o as the transmitted light in an empty spot of the viewing field. The measured transmittance is thus a composite of the transmittance plus the reflectance by the monitored mat section.

Results

Zonations and Microbial Processes in Intact Mat Samples

The cyanobacterial mat exhibited intense photosynthetic activity at a saturating irradiance of 413 μmol photons m^{-2} s^{-1} (Figure 1). Oxygen penetrated 5 mm below the mat surface, and O_2 concentration peaked at 3–4 times air saturation 1–2 mm below the mat surface. In the same zone a pH of up to 8.82 was measured, whereas pH decreased to pH 8.35 in the aphotic zone of the mat. The overlying water had a pH of 8.52. The photosynthetic activity was distributed in three major layers: a ~0.5 mm thick surface layer, and two ~1 mm thick layers situated at 1–2 mm and 2–3 mm depth below the mat surface, respectively.

Oxygenic photosynthesis could not be detected below 3 mm depth. Depth integration of porosity corrected gross photosynthesis rates amounted to 1.1494 nmol O_2 cm^{-2} s^{-1}, whereas the net flux of oxygen to the overlaying water and

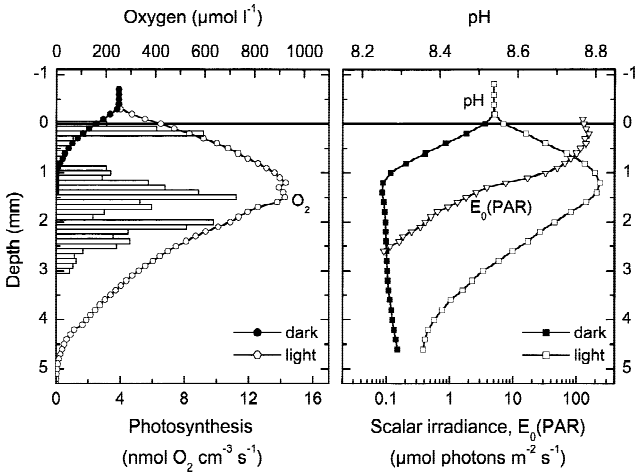

Fig. 1. Microprofiles of O_2, pH, quantum scalar irradiance, E_0(PAR), and gross oxygenic photosynthesis (bars) in a 7–8 mm thick cyanobacterial mat. Incident irradiance was 413 µmol photons m^{-2} s^{-1}.

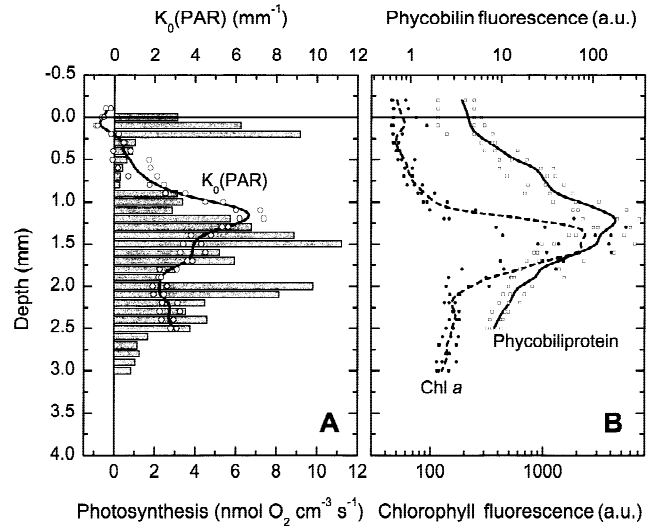

Fig. 2. Depth distribution of (A) oxygenic photosynthesis (bars) and the scalar irradiance diffuse attenuation coefficient, and (B) chlorophyll *a* and phycobiliprotein fluorescence in a 7–8 mm thick cyanobacterial mat. Solid lines indicate mean values of 2–3 profiles (indicated by symbols).

into the aphotic zone amounted to 0.1187 nmol O_2 cm^{-2} s^{-1} and −0.0338 nmol O_2 cm^{-2} s^{-1}, respectively. The net oxygen consumption of the illuminated mat could thus be estimated as (1.1494−0.1187) = 1.0307 nmol O_2 cm^{-2} s^{-1}, while the net oxygen consumption within the photic and aphotic zone was estimated as (1.1494 − (0.1187 + 0.0338)) = 0.9669 nmol O_2 cm^{-2} s^{-1} and (1.0307 − 0.9669) = 0.0338 nmol O_2 cm^{-2} s^{-1}, respectively. In the dark, i.e., ~30 min after darkening, oxygen only penetrated ~1 mm, and we calculated an areal oxygen consumption of 0.0578 nmol O_2 cm^{-2} s^{-1}. Volumetric rates of oxygen consumption were estimated by dividing areal rates by the depth of the reaction zone, assuming a constant activity within that zone. Volumetric oxygen consumption in the dark was 0.578 nmol O_2 cm^{-3} s^{-1}, while volumetric rates of oxygen consumption in the photic and aphotic zone amounted to 3.223 nmol O_2 cm^{-3} s^{-1} and 1.690 nmol O_2 cm^{-2} s^{-1}, respectively.

Scalar irradiance of photosynthetic available radiation in the mat, E_0(PAR), did not exhibit a monoexponential attenuation with depth. In the upper 0.5 mm of the mat, E_0(PAR) reached 100–150% of the incident downwelling irradiance because of intense scattering in the mat matrix of cells, exopolymers and carbonate precipitates (Figs. 1B and 2A). Scalar irradiance attenuation exhibited lowest values in a layer of exopolymers and carbonate precipitates ~0.2–0.8 mm below the mat surface. Highest light attenuation (K_0(PAR) ~5–7 mm^{-1}) was found in a predominantly cyanobacterial layer ~1.0–2.0 mm below the mat surface, where peaks of oxygenic photosynthesis, chlorophyll *a* and phycobiliproteins were also found (Fig. 2). The lower boundary of the net oxygenic zone 3 mm below the mat surface corresponded to E_0(PAR) levels of <0.1% of the incident irradiance.

Spectral radiance measurements in intact mat samples showed pronounced minima at wavelengths corresponding to absorption maxima of Chl *a,* carotenoids, and phycobiliproteins (Fig. 3) throughout the mat. Strong Bchl *a* absorption around 800 nm was found in layers >1.7 mm below the mat surface. Visible wavelength were attenuated >100 times more strongly than near infrared wavelengths of 730–750 nm.

Zonations in Thin Sections of Microbial Mat

Microscope spectrometry and fluorometry on freeze-sectioned mat samples allowed us to identify the vertical distribution of phototrophs. In Fig. 4 some representative absorbance spectra are shown. High absorbance of Chl *a* (440 and 675 nm) and phycobiliproteins (e.g., phycocyanin absorbance at 625 nm) over 0.2 mm thick zones revealed the presence of dense cyanobacterial layers mainly composed of *Calothrix*-, *Pseudanabaena*-, and *Phormidium*-like species. In deeper mat horizons, strong spectral signals of Bchl *a* (807 and 845 nm) and weaker signals of Bchl *c*(745–750 nm) were indicative of zones with purple and green photosynthetic

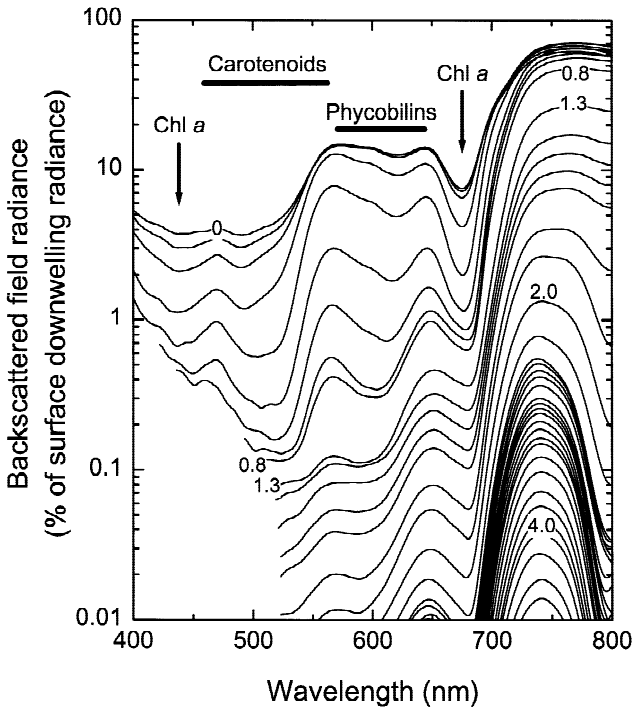

Fig. 3. Spectra of backscattered field radiance (in percent of downwelling surface radiance) measured in various depths below the surface of a 7–8 mm thick microbial mat. Numbers on curves indicate depths below surface in millimeters, and curves represent measurements done in steps of 0.1 mm. Spectra between 0.8 and 1.3 mm are left out, because of a cohesive carbonate layer present around this depth horizon.

bacteria, respectively. These observations were also supported by measurements of fluorescence emission spectra at selected depths (Fig. 5). Characteristic (cf. [16]) fluorescence emission maxima for Chl *a* (685 nm), Bchl *c* (758–760 nm), and Bchl *a* (860–870 nm) were detected.

The depth distributions of photopigment absorbance generally showed a good agreement with the distribution of the photosynthetic biota. The latter was obtained by stereological analysis of transmission electron microscopy pictures of different thin sections of mat [11]. Whereas the oxygenic phototrophs, predominantly cyanobacteria, formed dense layers in the top 3 mm of the mat (Fig. 6A), the anoxygenic phototrophs exhibited a more patchy distribution of bacterial colonies (Fig. 6B), which were, however, found in several distinct layers. Highest absorbance values for Chl *a* (675 nm) and cyanobacterial phycocyanin (625 nm) were found in the upper mm of the mat and below 2 mm from the mat surface (Fig. 6A). Highest absorbance values for Bchl *a* (807 and 845 nm) and Bchl *c* (750 nm) were found below 3 mm depth, but ~0.5 wide bands of increased absorbance were also present in the upper 3 mm of the mat sample (Fig. 6B).

Discussion

New Techniques for Bio-optical Studies in Microbial Mats

Fine-scale studies of the depth distribution of phototrophs, their photopigments, and their photosynthetic activity in relation to the prevailing light field in microbial mats require minimally invasive techniques that do not disturb the fine structural laminations and the steep gradients of environmental variables present. In the present study we have applied a combination of microsensor techniques with light microscopy and microspectrometry.

Fiber-optic microprobes are valuable tools for fine-scale characterization of light fields and optical properties of microbial mats in combination with photosynthesis measurements [18–20, 22–24]. The depth distribution of phototrophs has mainly been inferred from the spectral signatures of characteristic photopigments in transmittance or absorbance spectra measured with fiber-optic microprobes at different depths within microbial mats [20, 29, 31].

It is demonstrated here that fluorescence characteristics of different photopigments can also serve as proxies for the distribution and relative biomass of different groups of phototrophs in microbial mats. We show the first microprofiles of chlorophyll *a* and phycobiliprotein fluorescence distribution measured in an intact microbial mat community at 100 μm spatial resolution (Fig. 2B) by use of fiber-optic microprobes coupled to sensitive fluorometers. Different types of photopigments can be measured by proper selection of excitation and emission wavelengths on the fluorometer. Previously, measurements of vertical pigment distributions at such a high spatial resolution could only be obtained by use of destructive methods in combination with subsequent pigment extraction and analysis [6, 8, 29, 30]. Our fluorescence measurements with fiber-optic microprobes yielded only relative measures of biomass, whereas most destructive methods are quantitative. Absolute determination of pigment concentrations with fiber-optic microprobes is in principle doable, but a proper calibration of such measurements is difficult because of the complex optical properties of microbial mats [20].

Besides its applicability for measuring relative biomass distribution in microscale, chlorophyll fluorescence analysis with fiber-optic microprobes also holds a large potential for direct measurements of photosynthetic performance. A fiber-optic microprobe has been used recently to assess PSII activity and photoinhibition in discrete layers of a thin leaf at 20–30 μm spatial resolution [35], and this technique can also be applied for microscale photosynthesis studies in

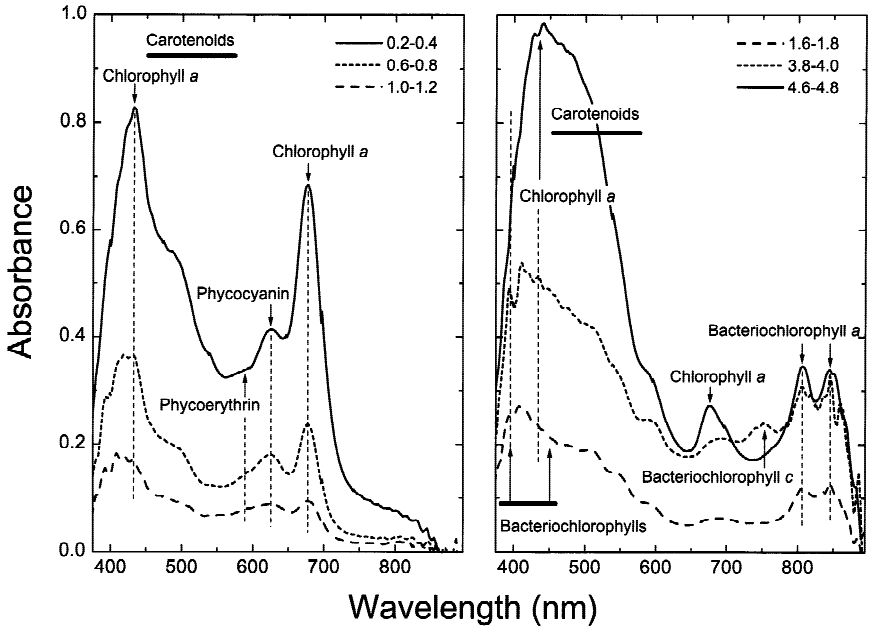

Fig. 4. Absorbance spectra obtained by microscope spectrometry on thin sections of a cyanobacterial mat. Absorbance was calculated for 200 μm depth intervals as indicated by the graph legend.

aquatic photosynthetic systems (M. Kühl, unpublished data).

A limitation of fiber-optic microprobes is the fact that the distribution of photosynthetic microorganisms can only be inferred from the spectral signatures of their photopigments, without any knowledge about the distribution of actual species and the microstructure within the mat. As with other microsensor techniques, the use of fiber-optic microprobes yields only relatively few point measurements, which need to be carefully evaluated against the microstructural heterogeneity of the investigated system [15]. Laser scanning confocal microscopy and reflectance spectroscopy allows noninvasive microstructural studies of intact translucent biofilms [25], but in sediments and microbial mats, which generally exhibit a high optical density, confocal microscopy can only reveal zonations within the upper 100–200 μm [46]. However, the use of new multiphoton confocal microscopy techniques, which are based on use of femtosecond pulses of NIR light, will probably enable analysis of deeper mat layers. Light as well as scanning and transmission electron microscopy has been used to study the microstructure and composition of microbial mats [4, 9, 13, 17, 28, 40]. Recently, light and transmission electron microscopy was used in combination with stereological analysis to obtain quantitative information on the distribution of biota [9, 11].

In this study, we combined light microscopy with microspectrometry for spectral measurements of absorbance and fluorescence on thin sections of microbial mat. This allowed us to correlate spectral signatures of photopigments to specific morphotypes of photosynthetic microorganisms positioned within the exopolymer matrix at known distance to the mat surface (Figs. 4–6). Previously, Garcia-Pichel and Castenholz [12] used a similar approach to study the presence and function of UV sunscreens in various cyanoabacteria. Our measurements were done at 40–200 μm spatial resolution, but because of the high sensitivity of our detector system the spatial resolution of this method is mainly governed by the microscope optics, and analysis of single cells is possible. We could also monitor dynamic changes in the optical properties of the microbial mats. A decrease in fluorescence intensity due to bleaching by UV and blue light excitation was, for example, much less pronounced in the surface layers of *Calothrix*-type cyanobacteria, which are known to contain UV sunscreens in their sheaths [12], as compared to almost immediate onset of bleaching in the subsurface layers dominated by *Pseudanabaena*- and *Phormidium*-type cyanobacteria.

Distribution of Photosynthesis and Phototrophic Microorganisms

We found a pronounced stratification of oxygenic photosynthetic activity into two or three distinct zones (Fig. 1) that generally matched the distribution of oxygenic phototrophs as inferred from the depth distribution of their photopigment absorbance and fluorescence characteristics, and by the depth distribution of PAR attenuation (Fig. 2). The zonation mirrors vertical changes in mat texture and distribution of oxygenic phototrophs found in an accompanying

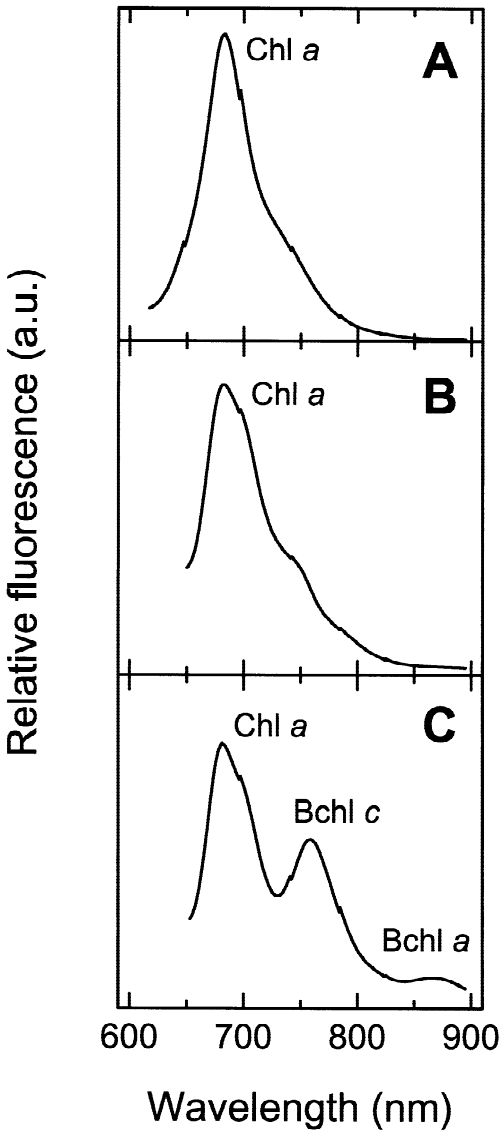

Fig. 5. (A, B) Fluorescence emission spectra measured ~0.3 mm (A) and ~2.9 mm (B) below the mat surface. A 20× microscope objective was used, and the field of view was ~200 μm. (C) Fluorescence emission spectrum measured ~3.9 mm below the mat surface with a 100× oil immersion microscope objective and a ~40 μm field of view. Fluorescence emission maxima corresponding to Chl *a* (683–685 nm), Bchl *c* (758–760 nm), and Bchl *a* (865–869 nm) are indicated on the graphs.

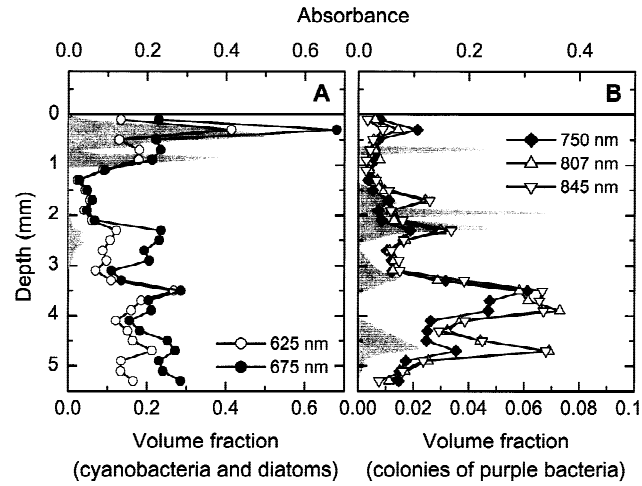

Fig. 6. Depth profiles of absorbance at 625 nm (phycocyanin), 675 nm (chlorophyll *a*), 750 nm (bacteriochlorophyll *c*), 807 nm, and 845 nm (bacteriochlorophyll *a*) measured by microcope spectrometry on thin sections of a cyanobacterial mat. Shaded areas represent the volume fraction of cyanobacteria and diatoms (A), and of colonies of purple bacteria (B) as determined by TEM on different thin sections (see [11] for details).

study (Fig. 6; [11]), where a relative loose surface layer dominated by *Calothrix*-type cyanobacteria was found on top of densely packed layers of different *Pseudanabaena* sp. *and Phormidium* sp. filaments. Only a few diatoms were found, and this explains the predominance of cyanobacterial spectral signatures in the various bio-optical data obtained in this study. The layers were mixed with and partly separated by carbonate precipitates, which probably resulted in the low photosynthetic activity measured in parts of the photic zone (Fig. 1). Layers containing photopigments of purple (Bchl *a*) and green (Bchl *a* and *c*) photosynthetic bacteria were mostly present below the oxygenic zone (Figs. 4, 5C), and the depth distributions inferred from the bio-optical data again showed a good correlation to previously measured distributions of anoxygenic photosynthetic bacteria (Fig. 6C). The colonies were dominated by *Thiocapsa*-like purple bacteria, but numerous other morphotypes of purple and green photosynthetic bacteria were found. Unfortunately, the spectral coverage of our measuring system (300–900 nm) did not allow us to demonstrate the presence of Bchl *b,* which absorbs around 1015 nm [30].

Especially in the upper 1 mm of the mat, carbonate within the matrix of exopolymers and cells also increased the scattering of light, resulting in a subsurface scalar irradiance peak of 150% of incident irradiance (Fig. 1). Consequently, attenuation of PAR was low, or even negative, in the upper 0.5 mm of the mat (Fig. 2A). A surface or subsurface maximum of scalar irradiance has been found in most microbial mats and sediments investigated [17, 19, 21, 22]. In deeper parts of the mat PAR was strongly attenuated with maximal attenuation coefficients of ~7 mm^{-1}. Attenuation coefficients of PAR determined in other microbial mats range from 2 to 12 mm^{-1} [21]. We did not quantify near-infrared scalar irradiance, but spectral radiance measurements indi-

cated a 100-fold lower attenuation of near infrared light as compared to visible wavelengths (Fig. 3), allowing anoxygenic photosynthetic bacteria to proliferate in deeper mat layers below the cyanobacteria [17, 19, 23, 27–29].

It is an interesting observation that removal of fauna and subsequent laboratory incubation under defined conditions of a constant diurnal light–dark cycle without any other imposed daily or seasonal variation (cf. [8]) leads to formation of mats that are similar in both function and structure to natural laminated microbial mats. The mats developed at an accretion rate of ~2–3 mm $year^{-1}$ into thick microbial communities that are stable over at least 3 years, i.e., the present age of the mats. Grazing and bioturbation by infauna must therefore be a major factor impeding the formation of microbial mats in most recent coastal environments. The fact that a pronounced vertical stratification of different photosynthetic microorganisms developed within a laminated matrix of exopolymers and carbonate layers in our mats indicates that light and the photobiological adaptations of microorganisms to light are indeed the major driving forces in formation of photosynthetic microbial mats, even in the absence of seasonally triggered variations in environmental variables and microbial populations.

Enhanced O_2 Consumption in the Light

Oxygen consumption within the mat was stimulated in the light. Although a higher areal oxygen consumption in light may be due to alleviation of diffusion limitation and the five-fold deeper oxygen penetration in light as compared to dark conditions, the enhancement of volumetric oxygen consumption in both the photic and aphotic zones points to other mechanisms. Volumetric oxygen consumption rates were ~5.5 times higher within the photic zone in light as compared to the oxygen consumption of darkened mats. Volumetric oxygen consumption rate in the aphotic zone of the illuminated mat was ~2.9 times higher than oxygen consumption in the darkened mat. Earlier studies attributed the apparent stimulation of oxygen consumption in illuminated biofilms and microbial mats to a combination of photorespiration and enhanced heterotrophic activity based on excretion of photosynthates in light [2, 7, 15, 21], and due to reoxidation of reduced organic and inorganic pools accumulating during periods of darkness [10, 45].

From our data we cannot judge the quantitative importance of the above-mentioned processes involved in enhanced oxygen consumption of illuminated mats. A biogeochemical study of the same albeit younger mat showed that a large fraction of the enhanced O_2 consumption could be due to reoxidation of reduced metabolic end products (e.g., reduced sulfur pools) accumulated during darkness [10]. However, preliminary sulfide measurements in the present mat only showed low sulfide levels (<30–50 μM) below 5–6 mm depth in both light and dark incubated mats (data not shown). We investigated ~1–1.5 cm deep subsamples of microbial mat in our study, and this apparently left out the major sulfide production zone present in deeper reduced sediment layers below the mat. Quantification of the biota in the mat showed highest bacterial numbers in layers of high density of phototrophs, and also showed a close structural association between bacteria and phototrophs at the level of single cells [11]. Furthermore, a recent study of the two-dimensional oxygen dynamics in a hypersaline microbial mat showed a spatial distribution of microsites with high oxygen consumption surrounding sites of high oxygen production [15]. Thus, there is both functional and microstructural evidence for efficient cross-feeding of heterotrophs by excretion of photosynthates in microbial mats. Whether such cross-feeding of heterotrophs also involves alleviation of CO_2 limitation for the autotrophs by the enhanced respiration remains to be shown.

Acknowledgments

This study was supported by grants from the Danish Natural Science Research Council to MK and TF. Anni Glud, Jeanne Sjøland Handest, and Ilse Duun are thanked for their careful technical assistance. We thank Unisense Aps. (Denmark) for providing the pA meter, and PyroImagination (Denmark) for providing the data acquisition and instrument control software used in this study.

References

1. Broecker WS, Peng TH (1974) Gas exchange rates between air and sea. Tellus 26:21–35
2. Canfield DE, Des Marais DJ (1993) Biogeochemical cycles of carbon, sulfur, and free oxygen in a microbial mat. Geochim Cosmochim Acta 57:3971–3984
3. Cohen Y, Rosenberg E (1989) Microbial Mats. American Society for Microbiology, Washington DC
4. D'Amelio E, D'Antoni, Cohen Y, Des Marais DJ (1989) Comparative functional ultrastructure of two hypersaline submerged cyanobacterial mats: Guerrero Negro, Baja California Sur, Mexico, and Solar Lake, Sinai, Egypt. In: Cohen Y, Rosenberg E (eds) Microbial Mats: Physiological Ecology of Benthic

Microbial Communities. American Society for Microbiology, Washington, DC, pp 97–113
5. Des Marais DJ (1995) The biogeochemistry of hypersaline microbial mats. Adv Microb Ecol 14:251–274
6. Dodds WK (1989) Microscale vertical profiles of N_2 fixation, photosynthesis, O_2, chlorophyll *a*, and light in a cyanobacterial assemblage. Appl Environ Microbiol 55:882–886
7. Epping E, Jørgensen BB (1996) Light enhanced areal oxygen respiration in benthic phototrophic communities. Mar Ecol Progr Ser 139:193–203
8. Fenchel T (1998) Formation of laminated cyanobacterial mats in the absence of benthic fauna. Aquat Microb Ecol 14:235–240
9. Fenchel T (1998) Artificial cyanobacterial mats: structure and composition of the biota. Aquat Microb Ecol 14:241–251
10. Fenchel T (1998c) Artificial cyanobacterial mats: cycling of C, O and S. Aquat Microb Ecol 14:253–259
11. Fenchel T, Kühl M (2000) Artificial cyanobacterial mats: Growth, structure and vertical zonation patterns. Microb Ecol
12. Garcia-Pichel F, Castenholz RW (1991) Characterisation and biological implications of scytonemin, a cyanobacterial sheath pigment. J Phycol 27:395–409
13. Garcia-Pichel F, Mechling M, Castenholz RW (1994) Diel migrations of microorganisms within a benthic hypersaline mat community. Appl Environ Microbiol 60:1500–1511
14. Glud RN, Jensen K, Revsbech NP (1995) Diffusivity in surficial sediments and benthic mats determined by use of a combined N_2O–O_2 microsensor. Geochim Cosmochim Acta 59:231–237
15. Glud RN, Kühl M, Kohls O, Ramsing NB (1999) Heterogeneity of oxygen production and consumption in a photosynthetic microbial mat as studied by planar optodes. J Phycol 35:270–279
16. Govindjee Amesz J, Fork DC (1986) Light Emission by Plants and Bacteria. Academic Press, New York
17. Jørgensen BB, Revsbech NP, Cohen Y (1983) Photosynthesis and structure of benthic microbial mats: microelectrode and SEM studies of four cyanobacterial communities. Limnol Oceanogr 28:1075–1093
18. Jørgensen BB, Cohen Y, Des Marais DJ (1987) Photosynthetic action spectra and adaptation to spectral light distribution in a benthic cyanobacterial mat. Appl Environ Microbiol 53:879–886
19. Jørgensen BB, Nelson DC (1988) Bacterial zonation, photosynthesis, and spectral light distribution in hot spring microbial mats of Iceland. Microb Ecol 16:133–147
20. Kühl M, Lassen C, Jørgensen BB (1994) Optical properties of microbial mats: light measurements with fiber-optic microprobes. In: Stal LJ, Caumette P (eds) Microbial Mats: Structure, Development and Environmental Significance. NATO ASI Ser. G, Vol. 35, Springer, Berlin, pp 149–167
21. Kühl M, Glud RN, Ploug H, Ramsing NB (1996) Microenvironmental control of photosynthesis and photosynthesis-coupled respiration in an epilithic cyanobacterial biofilm. J Phycol 32:799–812
22. Kühl M, Lassen C, Revsbech NP (1997) A simple light meter for measurements of PAR (400–700 nm) with fiber-optic microprobes: application for P vs E measurements in microbenthic communities. Aquat Microb Ecol 13:197–207
23. Lassen C, Ploug H, Jørgensen BB (1992) Microalgal photosynthesis and spectral irradiance in coastal marine sediments of Limfjorden, Denmark. Limnol Oceanogr 37:760–772
24. Lassen C, Jørgensen BB (1994) A fiber-optic irradiance microsensor (cosine collector): application for in situ measurements of absorption coefficients in sediments and microbial mats. FEMS Microbiol Ecol 15:321–336
25. Lawrence JR, Korber DR, Hoyle BD, Costerton JW, Caldwell DE (1991) Optical sectioning of microbial biofilms. J Bact 173:6558–6567
26. Li YH, Gregory S (1974) Diffusion of ions in sea water and in deep-sea sediments. Geochim Cosmochim Acta 38:703–714
27. Lorenzen J, Glud RN, Revsbech NP (1995) Impact of microsensor-caused changes in diffusive boundary layer thickness on O_2 profiles and photosynthetic rates in benthic communities. Mar Ecol Progr Ser 119:237–241
28. Nicholson JA, Stolz JF, Pierson BK (1987) Structure of microbial mat at Great Sippewisset Marsh, Cape Cod, Massachusetts. FEMS Microbiol Ecol 45:343–364
29. Oren A, Kühl M, Karsten U (1995) An endoevaporitic microbial mat within a gypsum crust: zonation of phototrophs, photopigments, and light penetration. Mar Ecol Progr Ser 128:151–159
30. Pierson BK, Oesterle A, Murphy GL (1987) Pigments, light penetration and photosynthetic activity in the multi-layered microbial mats of Great Sippewissett salt marsh. FEMS Microbiol Ecol 45:365–376
31. Pierson BK, Sands VM, Frederick JL (1990) Spectral irradiance and distribution of pigments in a highly layered marine microbial mat. Appl Environ Microbiol 56:2327–2340
32. Pierson BK, Bauld J, Castenholz RW, D'Amelio E, Des Marais DJ, Farmer J, Grotzinger JP, Jørgensen BB, Nelson DC, Palmisano AC, Schopf JW, Summons RE, Walter MR, Ward DM (1992) Modern mat-building microbial communities: a key to the interpretation of proterozoic stromatolitic communities. In: Schopf JW, Klein C (eds) The Proterozoic Biosphere. Cambridge University Press, New York
33. Revsbech NP (1989) An oxygen microelectrode with a guard cathode. Limnol Oceaonogr 34:474–478
34. Schidlowski M, Hayes JM, Kaplan IR (1983) Isotopic inferences of ancient biochemistries: Carbon, sulfur, hydrogen, and nitrogen. In: Schopf JW (ed) Earth's Earliest Biosphere. Princeton University Press, Princeton, pp 149–186
35. Schreiber U, Kühl M, Klimant I, Reising H (1996) Measurement of chlorophyll fluorescence within leaves using a modified PAM fluorometer with a fiber-optic microprobe. Photosynth Res 47:103–109
36. Schopf JW (1998) Tracing the roots of the Universal Tree of Life. In: Brack A (ed) The Molecular Origin of Life. Cambridge University Press, Cambridge, UK, pp 336–362

37. Schopf JW, Klein C (1992) The Proterozoic Biosphere. Cambridge University Press, New York
38. Stal LJ, Caumette P (eds) (1994) Microbial Mats. Springer, Berlin
39. Stal LJ, Van Gemerden H, Krumbein WE (1985) Structure and development of a benthic marine microbial mat. FEMS Microbiol Ecol 31:111–125
40. Stolz JF (1990) Distribution of phototrophic microbes in the flat laminated mat at Laguna Figueroa, Baja California, Mexico. BioSystems 23:345–357
41. Van Gemerden H (1993) Microbial mats: A joint venture. Mar Geol 113:3–25
42. Van Gemerden H, Tughan CS, de Wit R, Herbert RA (1989) Laminated microbial ecosystems on sheltered beaches in Scapa Flow, Orkney Islands. FEMS Microbiol Ecol 62:87–102
43. Walter MR, Bauld J, Des Marais DJ, Schopf JW (1992) A general comparison of microbial mats and microbial stromatolites: bridging the gap between the modern and the fossil. In: Schopf JW, Klein C (eds) The Proterozoic Biosphere. Cambridge University Press, New York, pp 335–338
44. Ward DM, Castenholz RW (2000) Cyanobacteria in geothermal habitats. In: Potts M, Whitton B (eds) Ecology of Cyanobacteria. Kluwer, Dordrecht, pp 37–59
45. Wieland A, Kühl M (2000) Short term effects on oxygen and sulfide cycling in a hyper-saline cyanobacterial mat (Solar Lake, Egypt). Mar Ecol Prog Ser 197:87–102
46. Wiggli M, Smallcombe A, Backhofen R (1999) Reflectance spectroscopy and laser confocal microscopy as tools in the ecophysiological study of microbial mats in an alpine bog pond. J Microbiol Meth 34:173–182